

Probing the α -Helical Structural Stability of Stapled p53 Peptides: Molecular Dynamics Simulations and Analysis

Zuojun Guo¹, Udayan Mohanty¹, Justin Noehre², Tomi K. Sawyer², Woody Sherman³ and Goran Krilov^{1,*}

¹Department of Chemistry, Boston College, 2609 Beacon Street, Chestnut Hill, MA 02467, USA

²Aileron Therapeutics, Inc., 840 Memorial Drive, Cambridge, MA 02139, USA

³Schrodinger, Inc., 120 W 45th Street, 17th Fl., New York, NY 10036, USA

*Corresponding author: Goran Krilov, goran@strandls.com

Reactivation of the p53 cell apoptosis pathway through inhibition of the p53-hDM2 interaction is a viable approach to suppress tumor growth in many human cancers and stabilization of the helical structure of synthetic p53 analogs via a hydrocarbon cross-link (staple) has been found to lead to increased potency and inhibition of protein–protein binding (J. Am. Chem. Soc. 129: 5298). However, details of the structure and dynamic stability of the stapled peptides are not well understood. Here, we use extensive all-atom molecular dynamics simulations to study a series of stapled α -helical peptides over a range of temperatures in solution. The peptides are found to exhibit substantial variations in predicted α -helical propensities that are in good agreement with the experimental observations. In addition, we find significant variation in local structural flexibility of the peptides with the position of the linker, which appears to be more closely related to the observed differences in activity than the absolute α -helical stability. These simulations provide new insights into the design of α -helical stapled peptides and the development of potent inhibitors of α -helical protein–protein interfaces.

Key words: circular dichroism, drug design, hDM2, molecular dynamic simulations, p53, protein–protein interfaces, stapled peptide, α -helicity

Received 2 December 2009, revised 19 January 2010 and accepted for publication 24 January 2010

A renaissance of peptide drug discovery has emerged over the past several years. In particular, the identification of synthetically 'stapled' α -helical peptides having promising pharmacokinetic, metabolic stability, and cell-penetrating properties has sparked tremendous interest in their development for a plethora of therapeutic targets that have otherwise been deemed 'undruggable' by more conventional small-molecule strategies (1). To date, numerous examples of stapled peptides for varying therapeutic targets have been described, including p53 (2), BID BH3 (3,4), BAD BH3 (5), NOTCH (6), and HIV-1 capsid (7). Both single-turn ($i + 4 \rightarrow i$) and double-turn ($i + 7 \rightarrow i$) stapling chemistries are represented in these studies.

Synthetic p53 peptides incorporating double-turn stapling chemistry have been previously described (2) and have provided insight to the evolution of a prototype series of cell-penetrating and *in vitro* biologically effective lead compounds. This series of peptides (Table 1) serves as the basis for the computational work presented here. These stapled p53 peptides have incorporated C α -methyl-amino acids having terminal olefin alkyl side chains of different lengths and chirality, such as (*S*)-CH₂₃-CH=CH₂ and (*R*)-CH₂₆-CH=CH₂, which upon metathesis form an all-carbon macrocycle via an olefin linkage (see compound **8**, Scheme 1). The structure–activity relationships of p53-stapled peptides **1–10** involve further amino acid modifications to decrease negative charge (i.e., Asp and Glu replacement by Asn and Gln, respectively) and facilitate cell penetration as well as point mutations to avoid nuclear export and ubiquitination (i.e., Lys replacement by Arg). In contrast, three key hydrophobic amino acids deemed critical for E3 ubiquitin ligase (MDM2) binding (i.e., Leu, Trp, and Phe as highlighted in stapled p53 peptide analogs **1–10**) were conserved throughout the series.

Importantly, the relationships between the structure and dynamic stability of stapled peptides are not well understood. Recently, an all-atom Monte Carlo folding simulation study comparing unmodified peptides derived from RNase A and BID BH3 with varying $i + 4 \rightarrow i$ and $i + 7 \rightarrow i$ stapling chemistry has been reported (8). Another investigation (9) led to the parameterization of a minimal, dynamic model reproducing the structural stability

Editor's invited manuscript to celebrate the 4th Anniversary of Chemical Biology & Drug Design.

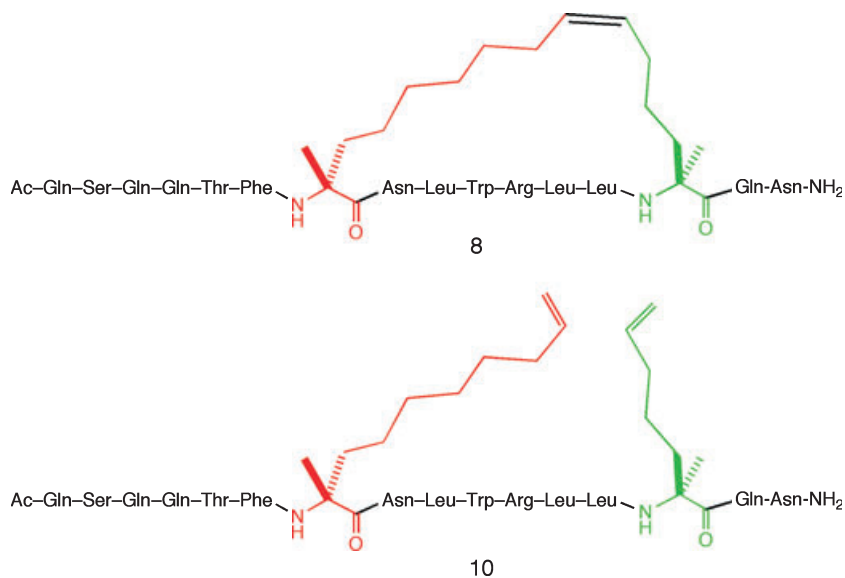
Table 1: The sequences of stapled α -helical p53 peptide analogs 1–10

Peptide	Sequence ^(a,b,c)
WT	Ac L S Q E T F S D L W K L L P E N NH ₂
1	Ac L S Q E T F S D X W K L L P E X NH ₂
2	Ac L S Q E X F S D L W K X L P E N NH ₂
3	Ac L S Q X T F S D L W X L L P E N NH ₂
4	Ac L S Q E T F X D L W K L L X E N NH ₂
5	Ac L S Q E T F X N L W K L L X Q N NH ₂
6	Ac L S Q Q T F X N L W R L L X Q N NH ₂
7	Ac Q S Q Q T F X N L W K L L X Q N NH ₂
8	Ac Q S Q Q T F X N L W R L L X Q N NH ₂
9	Ac Q S Q Q T A X N L W R L L X Q N NH ₂
10*	Ac Q S Q Q T F X N L W R L L X Q N NH ₂

^aX and X refer to Scheme 1 relative to the full chemical structure of peptide **8** (specifically, the two novel C_α-methyl-amino acids that are macrocyclized by olefin metathesis).

^bPeptide **10*** is a linear peptide (specifically, X refers to C_α-methyl-amino acid with (S)-CH₂₃-CH=CH₂ side chain, and X refers to C_α-methyl-amino acid with (R)-CH₂₆-CH=CH₂ side chain).

^cKey hydrophobic amino acids are highlighted in blue.


Scheme 1: Structures of stapled p53 analog peptide **8** and linear analog peptide **10**. A *cis*-olefin linkage is depicted for peptide **8** relative to synthesis and structural characterization by NMR and CD analysis at Aileron Therapeutics and will be described separately from this publication.

profile of a series of BH3-stapled peptides as a function of the cross-linking moiety.

Here, we use extensive molecular dynamics simulations to study a series of stapled α -helical peptides over a range of temperatures in solution. The peptides are found to exhibit substantial variations in

predicted α -helicities that are in good agreement with the experimental values (2). In addition, we find significant variation in local structural flexibility of the stapled peptides with the position of the linker, which appears to be more closely related to the observed differences in activity than the absolute α -helical stability. These simulations provide new insights into the design of α -helical

stapled peptides and the development of potent inhibitors of α -helical protein–protein interfaces.

Materials and Methods

Initial structures

All-atom structures of the 16-residue wild-type p53 peptide and the stapled analogs **1–10** were constructed using the Maestro package in an α -helical configuration. The olefin bridge was added manually, with the double bond placed in a *cis* configuration, as experimentally observed (based on synthesis and structural characterization by NMR and CD studies at Aileron Therapeutics and will be reported elsewhere). Protonation states were assigned to ionizable residues according to the pK_a based on pH = 7.0 using the Protein Preparation workflow in Maestro and the Epik module (10). Acetyl and carboxamide moieties were incorporated at the N- and C-termini of the peptide, respectively. Each peptide was then placed in a cubic cell, with size adjusted to maintain a minimum distance of 10 Å to the cell boundary, and soaked with a pre-equilibrated box of water using the System Builder module of the Desmond package (11,12). All overlapping solvent molecules were removed and an appropriate number of counter ions were added to maintain charge neutrality.

Molecular dynamics simulations

All molecular dynamics (MD) simulations were performed using the Desmond package (11,12). The OPLS 2005 force field (13,14) was used to model all peptide interactions, and the TIP3P model (15) was used for water. The particle-mesh Ewald method (16) (PME) was used to calculate long-range electrostatic interactions with a grid spacing of 0.8 Å. Van der Waals and short range electrostatic interactions were smoothly truncated at 9.0 Å. Nose–Hoover thermostats (17) were utilized to maintain the constant simulation temperature and the Martyna–Tobias–Klein method (18) was used to control the pressure. The equations of motion were integrated using the multistep RESPA integrator (19) with an inner time step of 2.0 fs for bonded interactions and non-bonded interactions within the short range cutoff. An outer time step of 6.0 fs was used for non-bonded interactions beyond the cutoff. Periodic boundary conditions were applied throughout.

The system was equilibrated with the default protocol provided in Desmond, which consists of a series of restrained minimizations and molecular dynamics simulations designed to slowly relax the system, while not deviating substantially from the initial protein co-ordinates. In short, two rounds of steepest descent minimization were performed with a maximum of 2000 steps and a harmonic restraint of 50 kcal/mol per Å² on all solute atoms. Next, a series of four molecular dynamics simulations were performed. The first simulation was run for 12 ps at a temperature of 10°K in the NVT (constant number of particles, volume, and temperature) ensemble with solute heavy atoms restrained with force constant of 50 kcal/mol per Å². Next, another 12 ps simulation was performed at 10°K with the same harmonic restraints, this time in the NPT (constant number of particles, pressure, and temperature) ensemble. A 24-ps simulation followed with the temperature raised to 300 K in the

NPT ensemble and the force constant retained. Finally, a 24-ps simulation was performed at 300 K in the NPT ensemble with all restraints removed. The above-mentioned default equilibration was followed by a 5000-ps NPT simulation to equilibrate the system. A 10-ns NPT production simulation was then run and configurations were saved in 4-ps intervals.

Additional simulations were run at high temperature and the final configuration was subjected to the above-mentioned protocol prior to the start of the 300-K production runs. For the high-temperature simulations, an initial set-up and equilibration period was performed as described earlier except for the final production stage. Each peptide was simulated at 500°K, which should provide sufficient kinetic energy to allow crossing of the relevant barriers separating the energy minima. A number of configurations (10–20) were selected from each high-temperature trajectory and used as a starting point for the 10-ns production simulations at 300 K described earlier. In total, 100–200 ns of sampling was performed for each peptide.

Replica exchange molecular dynamics simulations

The replica exchange molecular dynamics (REMD) approach (20) involves evolving a number of copies of the system in parallel at different temperatures and periodically exchanging the configurations between trajectories *i* and *j* with the probability $w_{ij} = \exp(-\Delta)$, where $\Delta \equiv (\beta_j - \beta_i) (E_j - E_i)$, and $\beta \equiv 1/k_B T$. This insures proper canonical sampling at all temperatures, with high-temperature simulations facilitating barrier crossings and low temperature simulations to explore local free energy minima. The systems were prepared and relaxed as described earlier. In each case, 64 replicas of the system were evolved in parallel for 15 ns at constant NVT, with temperatures evenly spaced between 300 and 600 K in approximately 4-K intervals. After the first 100 ps, replica exchanges between each pair of nearest neighbor trajectories were attempted every 12 ps to equilibrate the system. Following a 5-ns period, the configurations were saved in 1-ps intervals over the final 10 ns of each simulation, providing an aggregate 640 ns of sampling for each system. The exchange acceptance ranged from 22% to 55%, and convergence was confirmed by comparing ensemble averages computed separately over the first and last half of the production period.

Results and Discussion

We have performed extensive all-atom explicit solvent molecular dynamics simulations on a series of 10 stapled p53 peptide analogs previously synthesized and studied by Bernal *et al.* (2), as well as the wild-type peptide. The goal of this study was to determine how and to what extent the introduction of hydrocarbon cross-links at various locations in the sequence modifies the equilibrium conformational population of the peptides in solution. In particular, a crystal structure of the amino-terminal domain of MDM2 protein bound to the transactivation domain of p53, which the stapled peptides seek to mimic, shows the latter to be in a mostly α -helical conformation when bound to the receptor, allowing three hydrophobic amino acids on the hydrophobic side of the helix to adopt extended

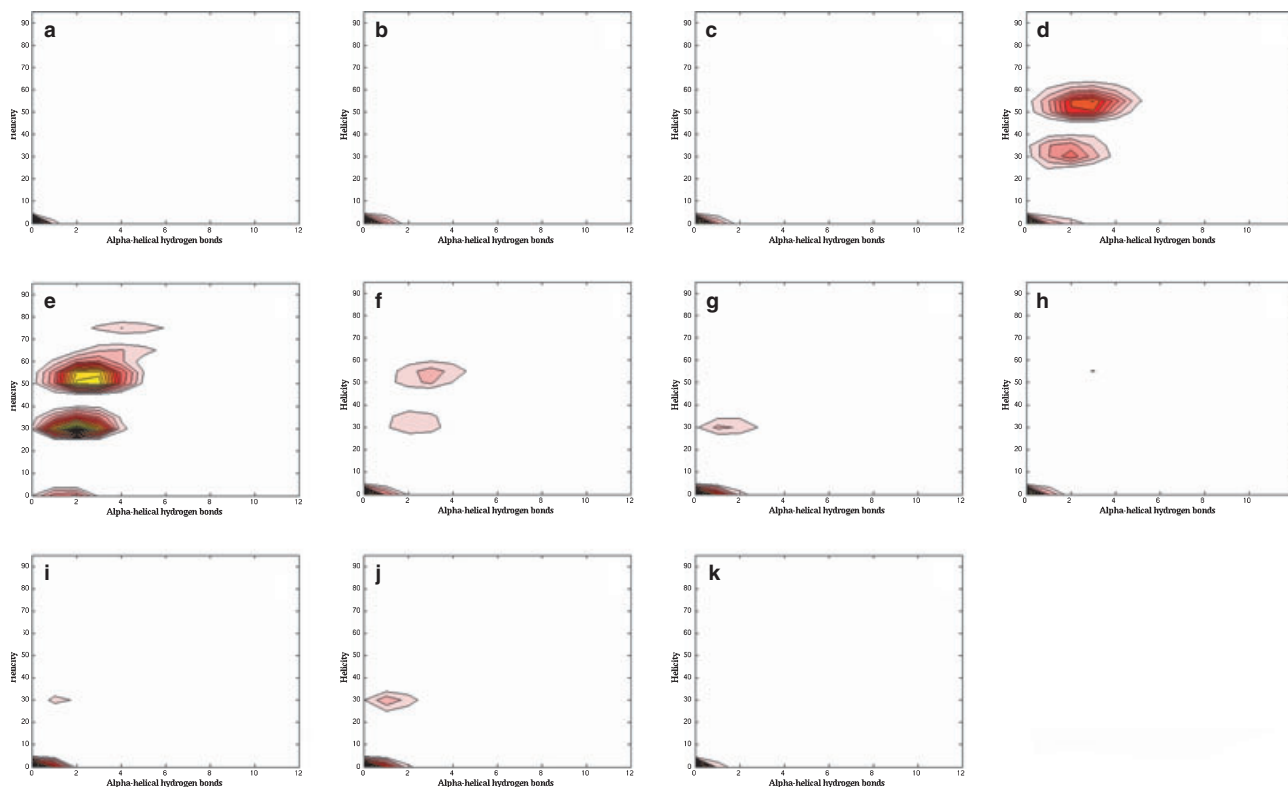


Figure 1: The contour plots of the conformational distribution of the p53 peptide analogs as a function of the number of backbone $i + 4 \rightarrow i$ α -helical hydrogen bonds and the percent α -helical content, for (a) **1**, (b) **2**, (c) **3**, (d) **4**, (e) **5**, (f) **6**, (g) **7**, (h) **8**, (i) **9**, (j) **10**, (k) wild type. Brighter color indicates higher intensity.

side-chain conformations and pack with each other (21,22). Circular dichroism (CD) measurements of free p53 in aqueous solution show a positive correlation between the degree of α -helical content and binding affinity of the peptides for hMDM2 (2). However, the α -helical content was found to vary widely across the series and some of the peptides with slightly decreased helical content exhibited significant activity in the low to mid nanomolar range, suggesting a more complex relationship between the peptide structures and binding activity. Also, intimately related to the intrinsic helical properties of the stapled p53 peptides is the C_{α} -methyl modification of the two amino acids that undergo metathesis to form the macrocycle. It is well-known that such C_{α} -methyl modification of linear peptides contributes to helicity (23–27), albeit such modifications have not been shown to confer the unique cell-penetrating properties of stapled peptides.

Structural distribution

One of the challenges of molecular dynamics of biomolecules is fully exploring the energetic landscape of the system. Biomolecules have complex potential energy profiles and simulations often get trapped for long periods of time in local minima because of the high energy barriers that may exist. In addition to not observing certain structures that may be biologically relevant, inadequate sampling also prevents recovering the correct thermodynamic distribution that is needed to correctly predict the energetics of the system. To improve sampling of the peptide, a

series of simulations were performed at high temperature (500 K) and snapshots were taken for multiple simulations at room temperature (300 K), as described in the Materials and Methods section. Because the active domain of p53 adopts a largely helical structure when bound to the MDM2 receptor, peptides that are not helical in solution would have to incur a conformational penalty to adopt the helical bound state conformation and therefore are hypothesized to be less active. Furthermore, the degree of helical content in the unbound state should correlate with binding activity if the conformational strain energy in the bound state is a limiting factor in the binding process. To better understand the structural profile of the peptides in the unbound state, we studied the helical content of the stapled peptides in solution.

There are numerous ways to define helical structure of the peptide chain. For example, proteins residues are typically classified as helical if their backbone dihedral angles ϕ and ψ lie in a narrow region of the Ramachandran diagram, with ϕ between -95° and -35° , and ψ between -15° and -70° (28). For α -helices, which are the predominant helical form in proteins, the sum of the ϕ and ψ angles on adjacent residues is $\sim -105^{\circ}$. This confines the dihedrals to a narrow strip with a slope close to -1 around an ideal α -helix geometry characterized by $(\phi, \psi) = (-60^{\circ}, -45^{\circ})$. For comparison, the sums of the above-mentioned angles were about -75° for the π -helix and -130° for the 3_{10} -helix (28). Helical conformations

Peptide	Sequence	Helicity	α -helical H-bonds
WT	Ac L S Q E T F S D L W K L L P E N NH ₂	2.0%	0.17
1	Ac L S Q E T F S D X W K L L P E X NH ₂	4.0%	0.44
2	Ac L S Q E X F S D L W K X L P E N NH ₂	0.0050%	0.17
3	Ac L S Q X T F S D L W X L L P E N NH ₂	1.8%	0.26
4	Ac L S Q E T F X D L W K L L X E N NH ₂	38%	2.0
5	Ac L S Q E T F X N L W K L L X Q N NH ₂	45%	2.5
6	Ac L S Q Q T F X N L W R L L X Q N NH ₂	26%	1.6
7	Ac Q S Q Q T F X N L W K L L X Q N NH ₂	15%	1.0
8	Ac Q S Q Q T F X N L W R L L X Q N NH ₂	22%	1.3
9	Ac Q S Q Q T A X N L W R L L X Q N NH ₂	12%	0.85
10	Ac Q S Q Q T F X N L W R L L X Q N NH ₂	11%	0.72

Table 2: Average helicity and number of α -helical hydrogen bonds from MD simulations at 300 K

are also recognized by a specific pattern of hydrogen bonds formed between the backbone acceptor carbonyl (C=O) of residue i and the backbone amine (NH) of another residue, including $i + 3$ (3_{10} -helix), $i + 4$ (α -helix), or $i + 5$ (π -helix). These definitions were used to analyze the conformational ensembles of stapled p53 peptide analogs.

In Figure 1, we plot the conformational population distribution as a function of percent α -helical content defined as the ratio of the number of helical residues to the total number of residues in the chain, and the number of α -helical ($i + 4 \rightarrow i$) hydrogen bonds. The α -helical nature of individual residues was assigned by the STRIDE program (29). The existence of hydrogen bonds was determined via a geometric criterion requiring a minimum donor (D)-to-(A) acceptor distance of 3.5 Å and a maximum A–H–D (acceptor–H–donor) angle of 30°. Interestingly, the helical population is predicted to be quite low for most peptides. In particular, **1**, **2**, **3**, **8**, and the WT p53 show a single pronounced peak at <5% helicity and 0–1 native hydrogen bonds, indicating minimal α -helical population. Compounds **4** and **5** each show two additional pronounced peaks, including a broad maximum centered at 30% helicity and 2 hydrogen bonds, and 50% helicity and 3 hydrogen bonds, respectively. These peaks are present to a lesser extent in **6**, and a small peak at 30% helicity and 1 hydrogen bond is observed for **7**, **9**, and the unstapled peptide **10**.

The average percent helicity for the entire population as calculated by STRIDE is given in Table 2. These are significantly lower than the helical content reported by Bernal *et al.* (10), which was estimated from CD measurements. One possibility for such a discrepancy may be because of a distortion of the helical structure away from the ideal α -helix geometry, indicating that the helix criteria used in the calculations mentioned earlier may be too stringent for direct comparison to experimental CD spectra. To investigate this further, we studied the distribution of the (ϕ, ψ) dihedrals for the p53 WT and ten stapled peptide analogs, as shown in Figure 2.

All distributions show a strong peak in the range $\phi = [-95, -50^\circ]$ and $\psi = [-50, -10^\circ]$, which is generally in the allowed α -helix

region of the Ramachandran diagram. Furthermore, these peaks display an oblong shape and lie roughly along a line with a slope of -1 in the (ϕ, ψ) plane, indicative of a periodic helical structure. The peptides known experimentally to have weak helical propensity, including **1**, **2**, **3**, and WT show significant populations in the two peaks located in extended β -sheet region (the upper left region of the Ramachandran plot), while strongly helical peptides such as **4** and **8**, which were found to be highly biologically effective (2), show most of the populations around the α -helical region. Still, the peaks are significantly broader than expected for an α -helix, indicating a distortion of the helical structure from ideal values.

In Table 3, we report the percentage of residues whose dihedral (ϕ, ψ) pairs were found to lie within a 30° band between (ϕ, ψ) = ($-95^\circ, -15^\circ$) and ($-35^\circ, -70^\circ$), characteristic of an α -helix. The percentages are generally higher than those reported by STRIDE, particularly for the weakly helical peptides and more in line with experimentally measured CD results. This supports the view that the default helical criteria in STRIDE is too stringent for direct comparison with CD spectra and that the helical structures adopted by the peptides are somewhat distorted from their ideal values. We also report the total number of backbone hydrogen bonds, which includes acceptor C=O to H–N donor pairings such as those from the 3_{10} -helices, π -helices, and β -hairpin turns, in addition to the α -helical backbone hydrogen bonds. The significantly larger values indicate a considerable contribution from the non- α -helical structural motifs to the equilibrium ensemble.

Next, we examine the conformational distribution of the stapled peptides as a function of temperature. This is useful because the degree of persistence of structural features in the peptide across a range of temperature provides insights into the stability of secondary structure and the energetic profile of the transition from structured to unstructured states. In Figure 3, we plot the average α -helicity computed by STRIDE as a function of temperature. The conformations of the peptide were harvested from separate 10-ns constant NPT simulations, following a 5-ns equilibration period performed at each temperature, ranging from 300 to 500 K (see Materials and Methods for details).

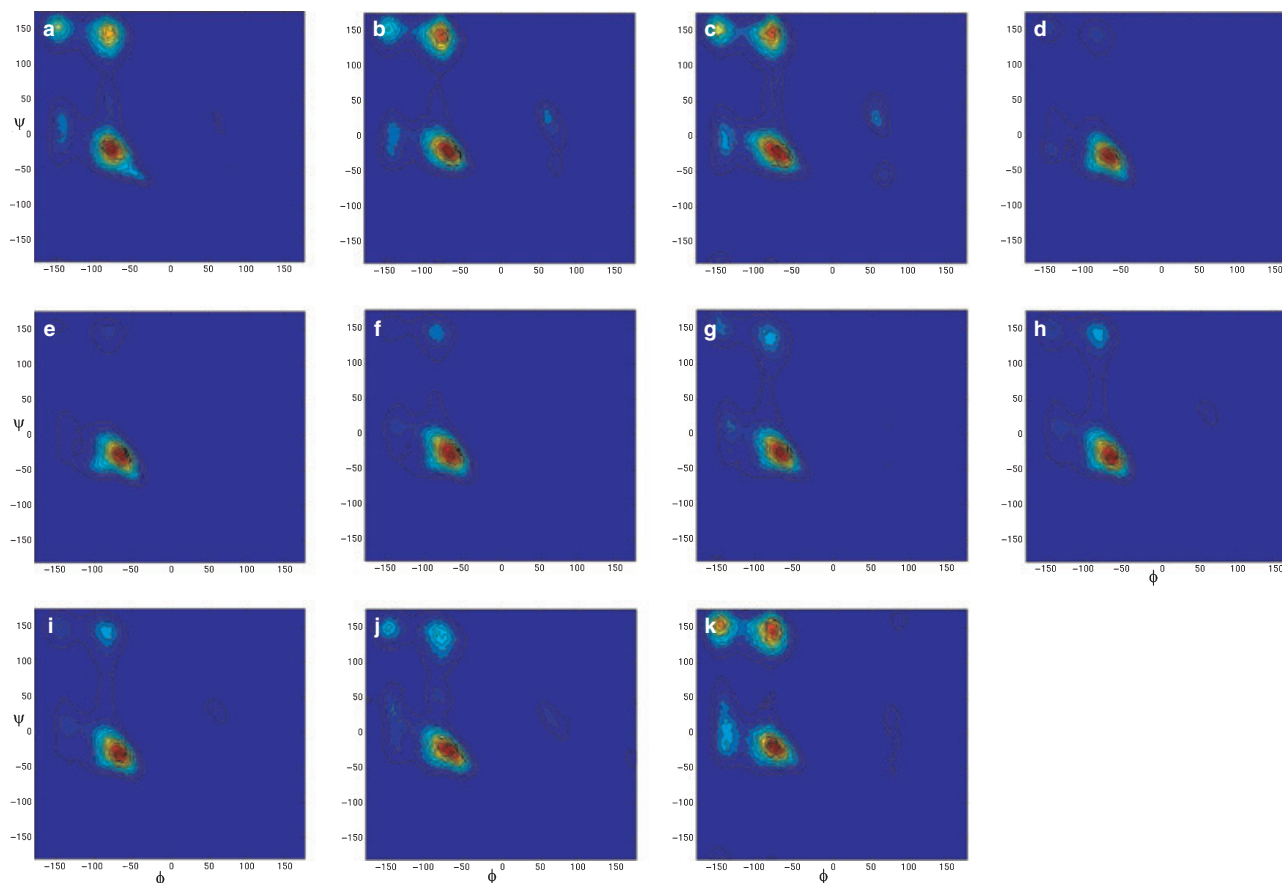


Figure 2: The Ramachandran plot of the distribution of the (ϕ, ψ) backbone dihedrals for (a) **1**, (b) **2**, (c) **3**, (d) **4**, (e) **5**, (f) **6**, (g) **7**, (h) **8**, (i) **9**, (j) **10**, and (k) WT. More red color indicates higher intensity.

Table 3: Fraction of backbone dihedrals in the helical region and the average number of backbone hydrogen bonds. Numbers in parentheses are only the α -helical hydrogen bonds

Peptide	Sequence	α -helical dihedrals	Backbone H-bonds
WT	Ac L S Q E T F S D L W K L L P E N NH ₂	14%	2.8 (0.2) ^a
1	Ac L S Q E T F S D X W K L L P E X NH ₂	20%	2.9 (0.2)
2	Ac L S Q E X F S D L W K X L P E N NH ₂	17%	2.9 (0.2)
3	Ac L S Q X T F S D L W X L L P E N NH ₂	17%	3.1 (0.1)
4	Ac L S Q E T F X D L W K L L X E N NH ₂	40%	4.7 (1.2)
5	Ac L S Q E T F X N L W K L L X Q N NH ₂	44%	5.6 (0.2)
6	Ac L S Q Q T F X N L W R L L X Q N NH ₂	35%	4.6 (0.6)
7	Ac Q S Q Q T F X N L W K L L X Q N NH ₂	28%	4.1 (1.1)
8	Ac Q S Q Q T F X N L W R L L X Q N NH ₂	32%	4.2 (2.0)
9	Ac Q S Q Q T A X N L W R L L X Q N NH ₂	24%	3.6 (0.3)
10	Ac Q S Q Q T F X N L W R L L X Q N NH ₂	24%	3.8 (1.5)

^aThe values in parenthesis indicate the standard error in the results.

The starting configuration in each simulation was an idealized α -helix. The comparison of the predicted α -helix melting curves shows that peptides with experimentally low helicity, including the wild-type p53 peptide **1** and **3**, display virtually complete melting

of the helix even at low temperature. Peptide **2** is predicted to have a relatively high helicity at room temperature, which is in disagreement with the low helicity observed in the experimental CD spectrum. However, the predicted melting curve decays rapidly with

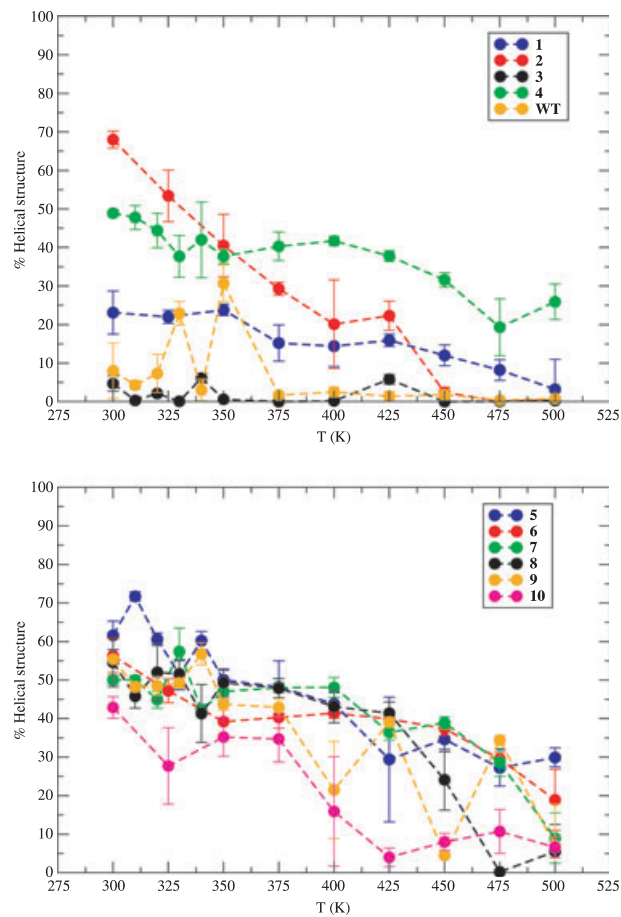


Figure 3: The helix melting curves showing the percent helical content as a function of temperature for (top) **1**, **2**, **3**, **4**, and the wild type; (bottom) **5**, **6**, **7**, **8**, **9**, **10**. The color coding is indicated in the legends.

temperature, indicating a co-operative unfolding process with a high energy barrier to initiate. Longer simulations at room temperature may yield different helicity predictions if this is a low frequency event that is not sampled statistically significantly with the current protocol. On the other hand, peptide **1** displays a flat curve, indicating that a low proportion of α -helical structure is maintained across a broad temperature range. This suggests a more stable, although not necessarily α -helical, structure.

Among the first group of peptides, **4** exhibits the highest helicity at room temperature ($\sim 50\%$), in agreement with experiment, and maintains this profile up to 450 K. The second series of peptides, **5** through **8**, demonstrate similar helical content at 300 K, in the range of 40–60%, with similar melting curves. In contrast with experimental data, **6**, which displays significantly weaker CD signal, exhibits a melting curve similar to the rest of the peptides in the series. Compounds **9** and **10** display the fastest decay of helical structure, in good agreement with experiment.

To further investigate the effect of the olefin linker on the secondary structure of the peptides, Figure 4 shows the per-residue

percent α -helicity, as computed by STRIDE, for the eleven stapled peptides at a series of temperatures. Several conclusions can be drawn from the plot. First, the per-residue helical profiles decay at a rate consistent with the average melting curves shown in Figure 3. However, helical content is not distributed evenly across the amino acid residues in the peptide. In each case, the region of the peptide with the highest helical content corresponds to the portion of the sequence spanned by the linker, although in some cases, such as **1** at 300 K, **9** at 400 K, and **10** at 425 K, helicity is found to be more evenly distributed over the sequence. Moreover, as the temperature increases, this region consistently maintains proportionately more helical content than the rest of the sequence. Hence, the linker is clearly predicted to induce helical structure formation but the effect is primarily local. A similar effect was observed by Kutchukian *et al.* (8) in their Monte Carlo study of the conformational distribution of stapled peptides derived from RNase A using a knowledge-based pseudo-potential, with the authors attributing the increased helix propensity of the spanned region to the stabilization of the folded state relative to the denatured conformation ensemble. This may explain the significant variations in the potency of the stapled peptides with linkers spanning different portions of the sequence and the lack of direct correlation between the experimental CD spectra and the peptide activity. Interestingly, Kutchukian *et al.* found that in case of a different sequence of stapled peptides derived from BID BH3, the spanned region is not predominantly helical, and a different, partially folded state is stabilized, indicating that the specific amino acid sequence of the peptide plays a significant role in determining the preference for helical conformations in conjunction with the location and length of the linker. We have observed such behavior in the helical propensity of **9**, which is one-half relative to **8**, even though the only difference is the replacement of a phenylalanine at position 8 with alanine, while the position of the staple and the spanned segment of the sequence is unaltered. Similarly, we observe that in case of peptides with most stable helices such as **8** and **4**, the helical region extends well past the segment spanned by the linker indicating a more comprehensive stabilization. This parallels the findings of Hamacher *et al.* (9) who, using a simplified Go model of the BH3 peptide, uncovered evidence of global dynamic stabilization of the cross-linked peptide helical structure in addition to the local stabilization imparted by the linker.

Finally, to explore whether the above-mentioned findings would be maintained with substantially more sampling, a subset of the peptides were subjected to an aggregate 640 ns of replica exchange molecular dynamics (REMD), as described in the Materials and Methods section. The computational resources required to run these simulations limited the number of peptides that could be run via REMD. Figures 5–8 show the helical conformational distribution, Ramachandran plots, per-residue helicity and the helix melting curves obtained from REMD simulations of peptides **4**, **8**, and WT, where the former two were selected for further study as they displayed a high degree of helicity by CD as well as high biological activity (2). In addition, peptide **8** showed a significantly lower helicity than observed experimentally in our constant temperature simulations. A comparison of Figures 5 and 6 with Figures 1 and 2 revealed both similarities and differences. There is consistency in the overall backbone

Probing the α -Helical Structural Stability of Stapled p53 Peptides

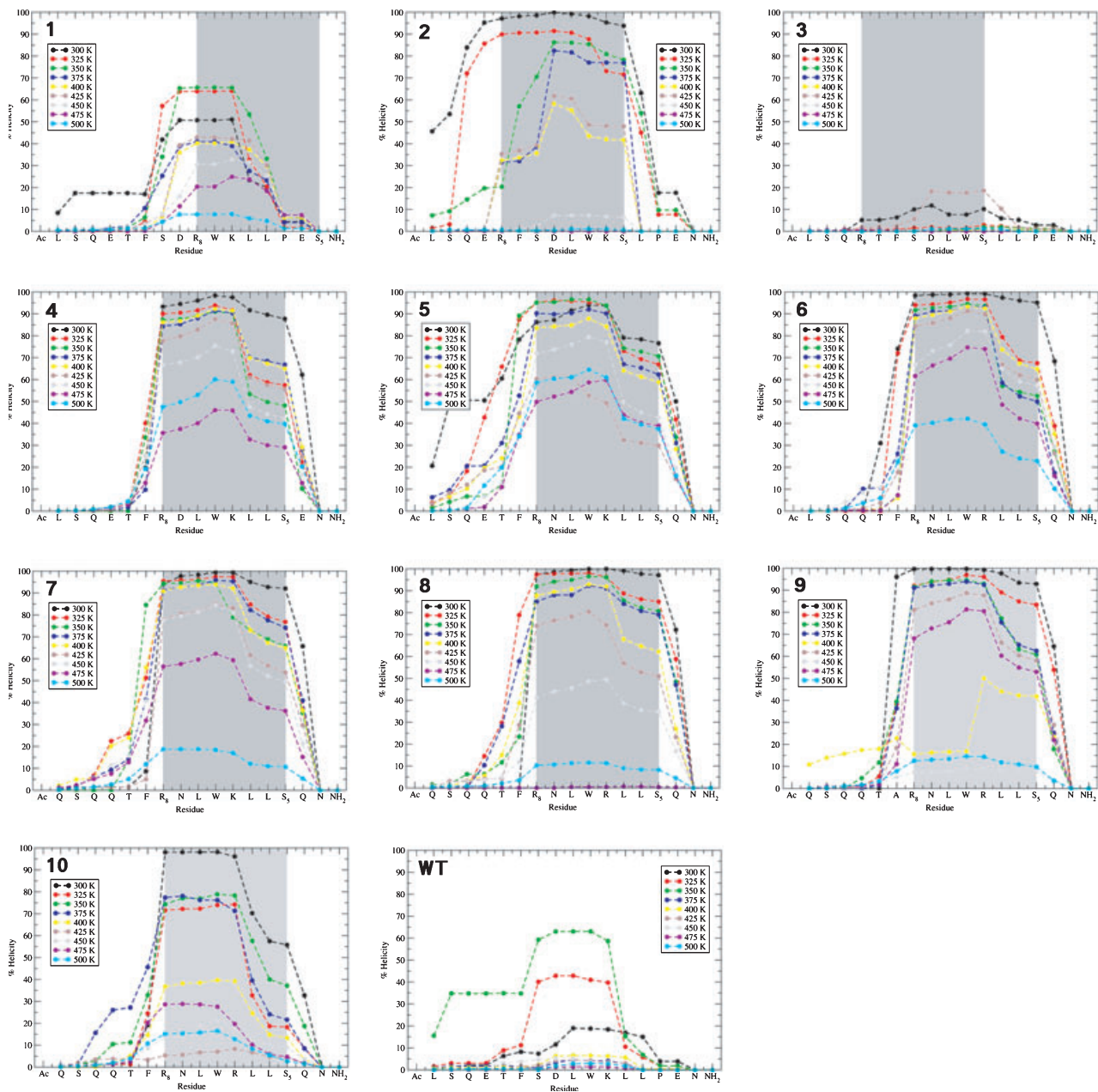


Figure 4: Percent helical occupancy for each of the 16 residues of the p53 peptide analogs, as a function of temperature for peptides **1**–**10** and WT p53. The data corresponding to a particular temperature are color coded as given in the legends. The shaded area indicates the residues spanned by the staple.

dihedral distribution, which supports that the conclusions from the shorter, non-REMD simulations relative to having enough sampling to generate reasonable predictions of α -helical content. However, the REMD simulations for peptide **8** show results that are more in line with the experimental values for α -helical content. Moreover, the conformational distribution of peptide **8** is now also observed to exhibit a multi-peak structure, indicating the presence of two partially folded states in addition to the full α -helical one.

To better illustrate the conformational differences between peptides, Figure 7 shows an overlay of backbone structures of the wild-type peptide and peptide **8**, sampled from principal population clusters identified in Figure 5. The superimposition was based on the α -carbon of the central six residues of the peptide. Also shown are an idealized α -helix of the WT peptide and the conformation of a 12-mer peptide in complex with MDM2, taken from the 3EQS crystal structure. It is evident that introduction of the macrocyclization (stapling) in peptide **8** generates sample conformations more closely

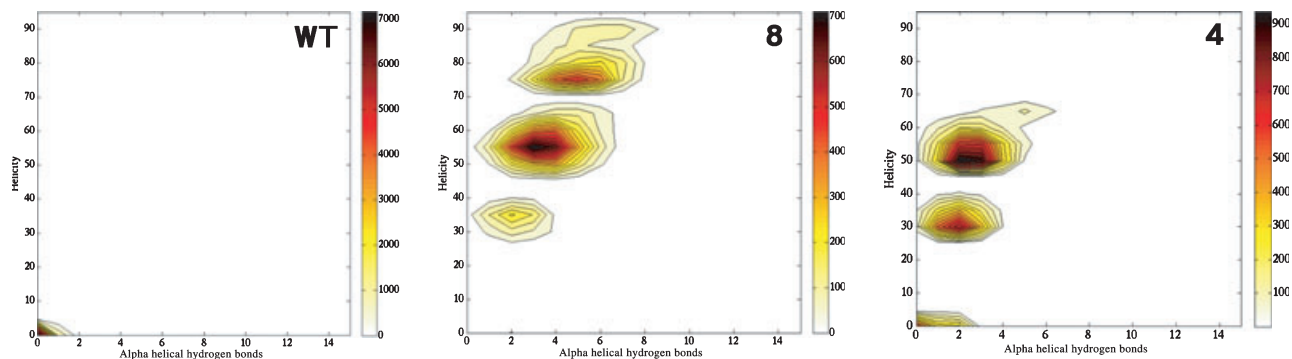


Figure 5: The contour plots of the conformational distribution of the WT p53 (left), **8** (middle), and **4** (right) peptides, as a function of the number of backbone $i \rightarrow i + 4$ α -helical hydrogen bonds and the percent α -helical content; computed from the replica exchange molecular dynamics (REMD) data. The Ramachandran plot of the distribution of the (ϕ, ψ) backbone dihedrals.

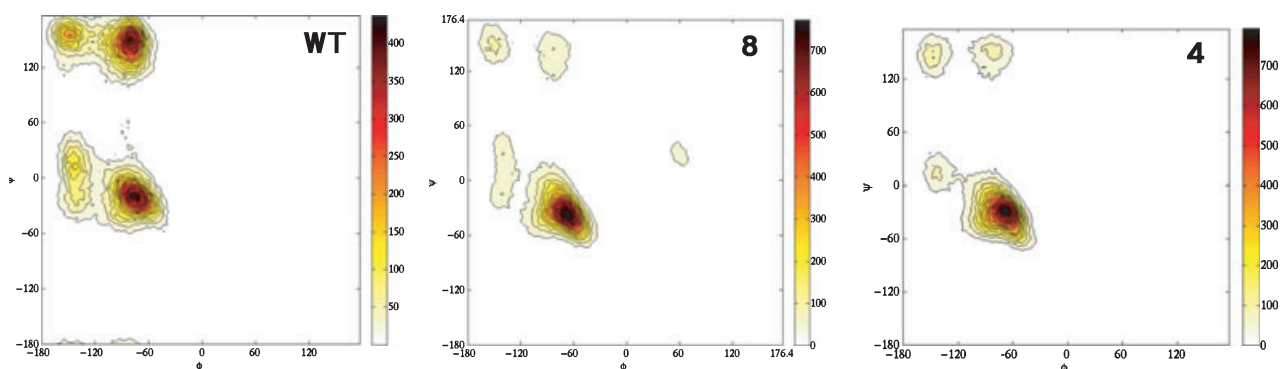


Figure 6: The Ramachandran plot of the distribution of the (ϕ, ψ) backbone dihedrals for the wild-type p53 (left), **8** (middle), and **4** (right) peptides, computed from the replica exchange molecular dynamics (REMD) data.

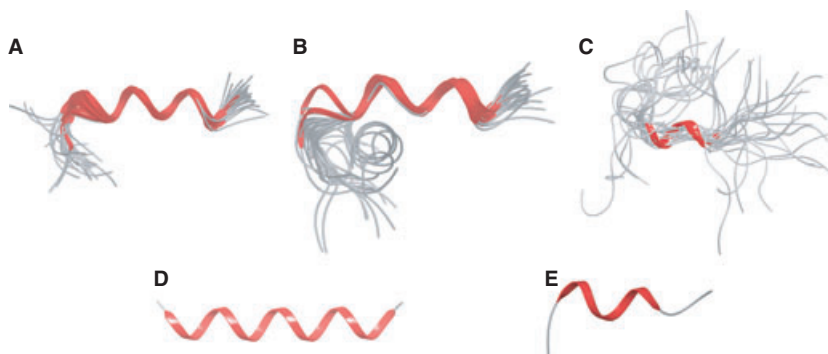


Figure 7: Backbone structures of peptide **8** sampled from the high helicity (A) and medium helicity (B) population cluster, and those of the WT p53 peptide (C), shown in comparison with the idealized p53 helix (D) and the conformation of p53 in crystal structure of the complex with MDM2 (E).

resembling an ideal helix (red), whereas the WT visits a plethora of random coil structures (gray), only infrequently visiting the partially folded helix observed in MDM2 complex crystal structure.

The melting curves in Figure 8 and the per-residue α -helicity shown in Figure 9 for the REMD simulations are qualitatively

similar to the data from shorter simulations, but quantitatively more in line with experimental results. This suggests that for qualitative understanding of α -helical content and relative helical content between peptides, it is sufficient to run shorter simulations. However, for quantitative predictions or comparisons with experiments, it is necessary to run long simulations, potentially

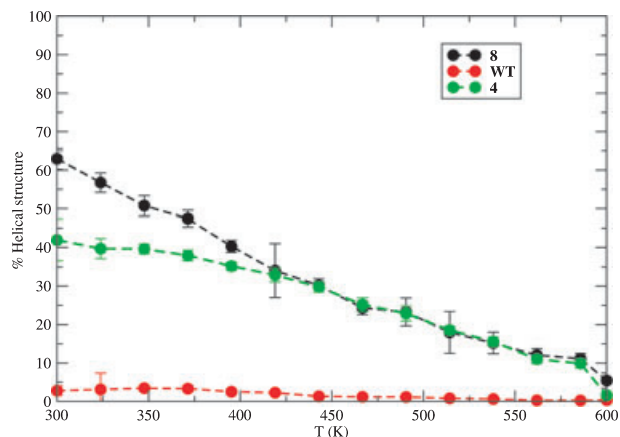


Figure 8: The helix melting curves computed from the replica exchange molecular dynamics (REMD) data, showing the percent helical content as a function of temperature for the wild-type p53 peptide, **8**, and **4**.

with enhanced sampling, as in the REMD simulations performed in this work. Animations of the REMD simulations are provided as Supporting Information. Movie S1 shows the wild-type p53 peptide and stapled p53 peptide **8**. Movie S2 shows the key hydrophobic side chains of stapled p53 peptide **8** that are important to its biological properties.

Conclusions and future directions

We have used extensive all-atom molecular dynamics simulations to study the structural distribution of a number of cross-linked analogs of the 16-residue transactivation domain of the p53 protein. The overall propensity to form α -helical structures was found to vary widely across the p53 peptide analog series and to depend both on the relative position of the macrocyclization (stapling) in the sequence as well as the specific amino acid substitutions. In general, all stapled p53 peptides except for **2** were found to have a higher α -helical content than the WT p53 peptide, which is in agreement with experimental CD measurements (2). The relative α -

helical propensity of most peptides was found to be in good qualitative agreement with experimental measurements, although our values are generally lower than those reported by Bernal *et al.* (2). This is partly because helical structures formed by the stapled peptides are somewhat distorted from the ideal α -helix geometry, and thus sometimes missed by the helix recognition algorithm in STRIDE. The latter is evident from the Ramachandran plots that show significant, but somewhat broader peaks in the α -helix region of the diagram. Computing the fraction of residues with (ϕ, Ψ) dihedrals within narrowly defined α -helical parameters gives helicities that are closer to the values estimated from CD measurements. REMD simulations performed for several peptides show that improved sampling results in predicted helicities that are very close to experimental values.

Interestingly, simulations of peptides **5** and **6** predict the helical content to be somewhat higher than suggested by experiments (2), as seen in Figure 1 and Table 2. While these peptides share the same position of the cross-link as **4**, they differ by substitution of several acidic residues with their amide counterparts, altering the total charge of the peptide. It is possible that the altered interactions with the specific solvent medium used in CD experiments reduce the helical propensity, which is not fully captured by our simulations. We also found that for several peptides, including **4**, **5**, **6**, and **8**, multiple partially folded states are populated at room temperature. Stabilization of such 'decoy states' by the staples was also observed by Kutchukian *et al.* (8), who pointed out that removal of these states may lead to more stable α -helical structures. This is particularly evident in the case of peptide **8**, where the most populated state is the partially folded state with mean helicity of 55% (Figure 5). Removal or destabilization of this state would likely lead to a population shift to a nearly fully helical state at mean helicity 75%.

The helical propensities were not distributed equally over the entire sequence. In most cases, the residues with the highest degree of helicity were found to be those spanned by the staple. In a few cases, particularly for **5** and **8**, significant helical content was observed in several residues outside of the linked region, while others with the identically positioned cross-link such as **4** do not share

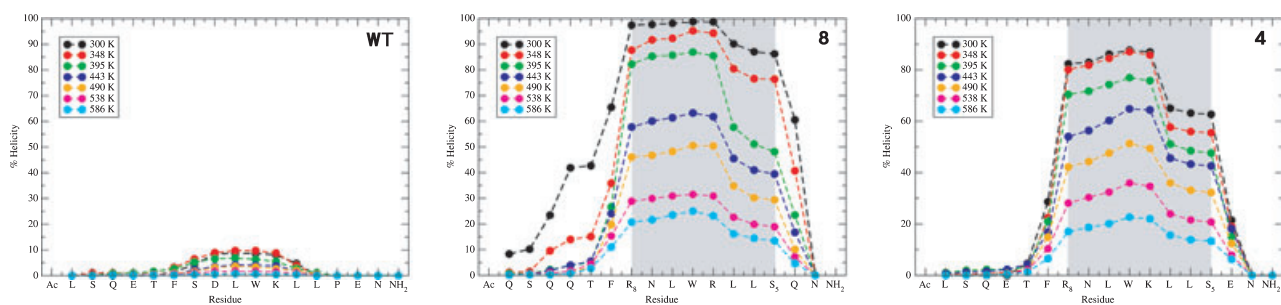


Figure 9: Percent helical occupancy for each of the 16 residues of WT (left), **8** (middle), and **4** (right) peptide analogs as a function of temperature, computed from the replica exchange molecular dynamics (REMD) data. The profiles corresponding to a particular temperature are color coded as shown in the legends. The shaded area indicates the residues spanned by the staple.

this trait. On the other hand, a distinct shoulder is observed in the per-residue helicity distribution for all peptides containing the LL motif in the spanned region. This suggests that, while helix formation is primarily because of local stabilization of helical geometry by the rigid linker, helical propensity is also strongly modulated by the details of the amino acid sequence of the peptide itself, and this should be taken into account relative to drug design a bioactive molecule. An existing question is to what extent the helical propensity is affected by the nature of the linker – its relative flexibility or rigidity, and conformational preference. We plan to investigate this relationship between the sequence-driven and linker-induced helical propensity in future studies. Finally, no attempt was made to correlate the properties of the peptides in the solution simulations with binding activity to MDM2 or to simulate the peptides in the bound state. Such work constitutes our ongoing desire to both understand and design stapled peptides having enhanced binding affinity to their respective therapeutic targets.

Acknowledgments

We would like to thank Dr Carl Elkin for helpful comments on the manuscript and Noeris Salam for making the PyMOL movies in the Supporting Information. This work was partially funded by the Guggenheim Fellowship awarded to U.M.

References

- Walensky L.D., Verdine G.L. (2007) The challenge of drugging undruggable targets in cancer: lessons learned from targeting BCL-2 family members. *Clin Cancer Res*;13:7264–7270.
- Bernal F., Tyler A.F., Korsmeyer S.J., Walensky L.D., Verdine G.L. (2007) Reactivation of the p53 tumor suppressor pathway by a stapled p53 peptide. *J Am Chem Soc*;129:2456–2457.
- Walensky L.D., Kung A.L., Escher I., Malia T.J., Barbuto S., Wright R.D., Wagner G., Verdine G.L., Korsmeyer S.J. (2004) Activation of apoptosis in vivo by a hydrocarbon-stapled BH3 helix. *Science*;305:1466–1470.
- Walensky L.D., Pitter K., Morash J., Oh K.J., Barbuto S., Fisher J., Smith E., Verdine G.L., Korsmeyer S.J. (2006) A stapled BID BH3 helix directly binds and activates BAX. *Mol Cell*;24:199–210.
- Daniel N.N., Walensky L.D., Zhang C.Y., Choi C.S., Fisher J.K., Molina A.J., Datta S.R. *et al.* (2008) Dual role of proapoptotic BAD in insulin secretion and β cell survival. *Nat Med*;14:144–153.
- Moellering R.E., Cornejo M., Davis T.N., Del Bianco C., Aster J.C., Blacklow S.C., Kung A.L., Gilliland D.G., Verdine G.L., Bradner J.E. (2009) Direct inhibition of the NOTCH transcription factor complex. *Nature*;462:182–188.
- Bhattacharya S., Zhang H., Debnath A.K., Cowburn D. (2008) Solution structure of a hydrocarbon stapled peptide inhibitor in complex with monomeric C-terminal domain of HIV-1 capsid. *J Biol Chem*;283:16274–16278.
- Kutchukian P.S., Yang J.S., Verdine G.L., Shakhnovich E.I. (2009) All-atom model for stabilization of α -helical structure in peptides by hydrocarbon staples. *J Am Chem Soc*;131:4622–4627.
- Hamacher K., Hübsch A., McCammon J.A. (2006) A minimal model for stabilization of biomolecules by hydrocarbon cross-linking. *J Chem Phys*;124:164907 (1–8)
- Shelley J.C., Cholleti A., Frye L.L., Greenwood J.R., Timlin M.R., Uchimaya M. (2007) Epik: a software program for pKa prediction and protonation state generation for drug-like molecules. *J Comp-Aided Mol Des*;21:681–691.
- Bowers K.J., Chow E., Xu H., Dror R.O., Eastwood M.P., Gregersen B.A., Klepeis J.L., Kolossvary I., Moraes M.A., Sacerdoti F.D., Salmon J.K., Shan Y., Shaw D.E. (2006) Scalable algorithms for molecular dynamics simulations on commodity clusters. In SC '06. Proceedings of the 2006 ACM/IEEE conference on Supercomputing. New York, USA.
- Desmond v2.2, Schrödinger, Inc.: Portland, OR.
- Jorgensen W.L., Maxwell D.S., Tirado-Rives J. (1996) Development and testing of the OPLS all-atom force field on conformational energetics and properties of organic liquids. *J Am Chem Soc*;118:11225–11236.
- Kaminski G.A., Friesner R.A., Tirado-Rives J., Jorgensen W.L. (2001) Evaluation and reparametrization of the OPLS-AA force field for proteins via comparison with accurate quantum chemical calculations on peptides. *J Phys Chem B*;105:6474–6487.
- Jorgensen W.L., Chandrasekhar J., Madura J.D., Impey R.W., Klein M.L. (1983) Comparison of simple potential functions for simulating liquid water. *J Chem Phys*;79:926–935.
- Essmann U., Perera L., Berkowitz M.L., Darden T., Lee H., Pedersen L.G. (1995) A smooth particle mesh Ewald method. *J Chem Phys*;103:8577–8593.
- Hoover W.G. (1985) Canonical dynamics: equilibrium phase-space distributions. *Phys Rev A*;31:1695–1697.
- Martyna G.J., Tobias D.J., Klein M.L. (1994) Constant pressure molecular dynamics algorithms. *J Chem Phys*;101:4177–4189.
- Humphreys D.D., Friesner R.A., Berne B.J. (1994) A multiple-time-step molecular dynamics algorithm for macromolecules. *J Phys Chem*;98:6885–6892.
- Sugita Y., Okamoto Y. (1999) Replica-exchange molecular dynamics method for protein folding. *Chem Phys Lett*;314:141–151.
- Kussie P.H., Gorina S., Marechal V., Elenbaas B., Moreau J., Levine A.J., Pavletich N.P. (1996) Structure of the MDM2 oncoprotein bound to the p53 tumor suppressor transactivation domain. *Science*;274:948–953.
- Frishman D., Argos P. (1995) Knowledge-based protein secondary structure assignment. *Proteins*;23:566–579.
- Formaggio F., Pegoraro S., Crisma M., Valle G., Toniolo C., Précioux G., Boesten W.H., Schoemaker H.E., Kamphuis J. (1993) Reverse relationship between α -carbon chirality and helix handedness in (α -Me)Phe peptides. *J Biomol Struct Dyn*;10:919–931.
- Kubelka J., Silva R.A., Keiderling T.A. (2002) Discrimination between peptide 3(10)- and α -helices. Theoretical analysis of the impact of α -methyl substitution on experimental spectra. *J Am Chem Soc*;124:5332–5332.
- Toniolo C., Formaggio F., Tognon S., Broxterman Q.B., Kaptein B., Huang R., Setnicka V., Keiderling T.A., McColl I.H., Hecht L., Barron L.D. (2004) The complete chiro-spectroscopic signature of the peptide 3(10)-helix in aqueous solution. *Biopolymers*;75:32–45.

26. Moretto A., Crisma M., Kaptein B., Broxterman Q.B., Toniolo C. (2006) N-methylation of N α -acylated, fully C α -methylated, linear, folded peptides: synthetic and conformational aspects. *Biopolymers*;84:553–565.
27. De Poli M., Moretto A., Crisma M., Peggion C., Formaggio F., Kaptein B., Broxterman Q.B., Toniolo C. (2009) Is the backbone conformation of C α -methyl proline restricted to a single region? *Chemistry*;15:8015–8025.
28. Lesk A. (2001) *Introduction to Protein Architecture*. Oxford, UK: Oxford University Press.
29. Toniolo C., Crisma M., Bonora G.M., Klajc B., Lelj F., Grimaldi P., Rosa A. *et al.* (1991) Peptides from chiral C α , α -disubstituted glycines. Synthesis and characterization, conformational energy computations and solution conformational analysis of C α -methyl, C α -isopropylglycine [(α -Me)Val] derivatives and model peptides. *Int J Pept Protein Res*;38:242–252.

Supporting Information

Additional supporting information may be found in the online version of this article.

Movie S1. Replica exchange molecular dynamics on p53 wild-type peptide and stapled p53 peptide 8.

Movie S2. Replica exchange molecular dynamics on stapled p53 peptide 8 showing key hydrophobic side chains that are important to its biological properties.

Please note: Wiley-Blackwell is not responsible for the content or functionality of any supporting materials supplied by the authors. Any queries (other than missing material) should be directed to the corresponding author for the article.